Interpenetration and stagnation in colliding laser plasmas

K. F. Al-Shboul,[1,2] S. S. Harilal,[1,a)] S. M. Hassan,[1] A. Hassanein,[1] J. T. Costello,[3] T. Yabuuchi,[4] K. A. Tanaka,[4] and Y. Hirooka[5]
[1]*Center for Materials Under eXtreme Environment, School of Nuclear Engineering, Purdue University, West Lafayette, Indiana 47907, USA*
[2]*Department of Nuclear Engineering, Jordan University of Science and Technology, Irbid 22110, Jordan*
[3]*School of Physical Sciences and NCPST, Dublin City University, Dublin 9, Ireland*
[4]*Graduate School of Engineering, Osaka University, Yamada-oka 2-1, Suita, Osaka 5650871, Japan*
[5]*National Institute for Fusion Science, 322-6 Oroshi, Toki, Gifu, Japan*

(Received 14 October 2013; accepted 12 December 2013; published online 7 January 2014)

We have investigated plasma stagnation and interaction effects in colliding laser-produced plasmas. For generating colliding plasmas, two split laser beams were line-focused onto a hemicircular target and the seed plasmas so produced were allowed to expand in mutually orthogonal directions. This experimental setup forced the expanding seed plasmas to come to a focus at the center of the chamber. The interpenetration and stagnation of plasmas of candidate fusion wall materials, viz., carbon and tungsten, and other materials, viz., aluminum, and molybdenum were investigated in this study. Fast-gated imaging, Faraday cup ion analysis, and optical emission spectroscopy were used for diagnosing seed and colliding plasma plumes. Our results show that high-Z target (W, Mo) plasma ions interpenetrate each other, while low-Z (C, Al) plasmas stagnate at the collision plane. For carbon seed plasmas, an intense stagnation was observed resulting in longer plasma lifetime; in addition, the stagnation layer was found to be rich with C_2 dimers. © *2014 AIP Publishing LLC*. [http://dx.doi.org/10.1063/1.4859136]

I. INTRODUCTION

Recently, laser-produced colliding plasmas have found potentially attractive applications in the field of X-ray lasers, pulsed-laser deposition (PLD), laser ion sources, and in the generation of astrophysical objects in the laboratory frame.[1–9] Despite extensive experimental and theoretical progress in the dynamics of single laser produced plasmas (LPPs), little attention has been paid to the study of the nature and dynamics of laser-produced colliding plasmas even though several new applications are emerging. Several target geometries and configurations[10–14] have been used for generating and investigating colliding plasmas where a number of observations were reported and parameters determined such as changes in the kinetic energy of the ablated species and the degree of their ionization.[15,16] Previous studies showed that charge-changing collisions among species in the plume will happen during such interpenetration.[17,18] Most of the reported colliding plasma results focused on generating astrophysical objects in the laboratory frame, which require high temperature and high density plasma schemes and hence higher laser intensities were used ($>10^{13}$ W cm^{-2}).[19,20]

Colliding plasma schemes are also useful for understanding plasma screening effects in fusion chambers. For operating fusion reactors with high implosion repetition rates, the chamber should be cleaned to near pristine condition after each implosion.[21] In such extreme environments, the reactor wall materials will be exposed to short x-ray pulses and fusion generated fragments and the chamber walls are believed to have to withstand a total flux density of ~10 J/cm^2/pulse.[22] This will cause ablation of the wall material leading to plasma formation and collision among the core and wall plasmas within the reactor chamber. Exposed to such extreme fluxes, plasma-facing components (PFC) are expected to eject particles and generate stagnation plasma clouds, aerosols, or clusters, depending on the choice of material. Such extremely high exposure levels will limit the wall lifetime and potentially act as a serious impediment to the achievement of high implosion rates due to laser light scattering or deflection by the potential colliding plasma clouds. Recent studies showed that colliding plasma experiments can be used to simulate aerosol formation in chamber walls.[23–25]

In this article, we used a colliding plasma experimental scheme to investigate the collision and plasma screening effects similar to PFC ablation in fusion reactors. The seed plasmas were generated using 1064 nm, 6 ns Nd:YAG laser pulses. The interpenetration and stagnation of plasmas of candidate fusion wall materials, viz., carbon and tungsten, and other materials, viz., aluminum and molybdenum were investigated in this study. The colliding plasmas of high-Z metals (W and Mo) did not result in stagnation and their seed plasmas were simply found to interpenetrate each other. On the other hand, Al plasmas showed interpenetration at early times followed by a moderate stagnation. However, in the case of carbon, an intense stagnation layer was observed in the colliding seed plasmas. Therefore, more detailed spectroscopic studies have been carried out in the carbon stagnation layer to study electron density and temperature, C_2 formation and vibrational temperature, and other stagnation layer properties.

II. EXPERIMENTAL SETUP

A schematic of the experimental setup is shown in Fig. 1(a). The seed plasmas were generated using 1064 nm,

a)hari@purdue.edu

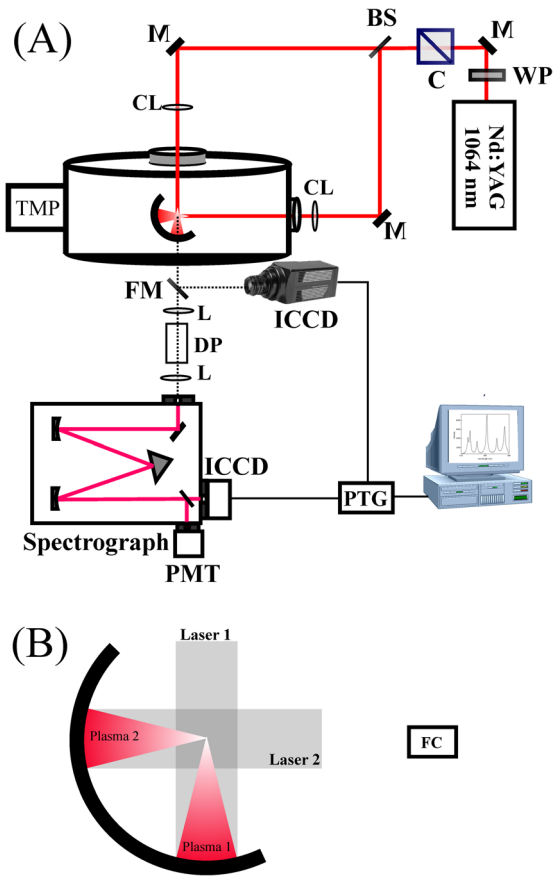

FIG. 1. The schematic of the experimental setup is given in (A). The Nd:YAG laser beam was split into two beams with the help of a beam splitter. The laser beams were focused onto the target using cylindrical lenses (CL). The side window of the vacuum chamber was used for collecting light to permit optical emission spectroscopy and fast gated imaging. The position of the FC with respect to seed plasmas is shown in (B). The two laser beams and seed plasmas are also identified in (B) (M, mirror; BS, 50:50 beam splitter; TMP, turbomolecular pump; PMT, photomultiplier tube; PTG, programmable timing generator; WP, waveplate; C, polarizing cube; L, lens; DP, dove prism; FM, folding mirror).

6 ns pulses at a pulse repetition rate of 10 Hz provided by a Nd:YAG laser. The laser beam energy was controlled using a combination of a waveplate and a cube polarizer and split into two equal energy parts using a beam splitter. Different target materials were used, viz., C, Al, Mo, and W, in this study. Each of these materials was carefully machined into the form of a hemi-circular shaped target (radius $\sim$ 1.5 cm). Both split laser beams were line focused onto the target surface horizontally (along the target curvature), using cylindrical lenses with f = 40 cm, each yielding a 1 cm $\times$ 0.01 cm spot with a laser irradiance at the foci $\sim 8.3 \times 10^8$ W cm^{-2}. Both beams arrive at the target at the same time. This peculiar target geometry along with line focusing will lead to focusing of the seed plasmas approximately in the center of the hemispherical target focal point (Fig. 1(b)). The target was continuously translated inside a vacuum chamber (pressure $\sim 10^{-5}$ Torr) using a mechanical stage to provide a fresh surface for each laser shot.

Various plasma diagnostic tools were used for analyzing seed and colliding plasma properties including optical emission spectroscopy, intensified charged coupled device (ICCD) fast gated imaging, Faraday Cup (FC), etc., more details of the associated instrumentation can be found elsewhere.[26,27] The self-emission from the plasma was collected using appropriate optics and focused onto the slit of a 0.5 m triple grating Czerny-Turner spectrograph. A dove prism was used to rotate the seed plasma and stagnation layer plume images so that they expanded up along the slit height of the spectrograph. The dispersed light was detected by an ICCD, which was attached to the spectrograph. The ICCD camera was also utilized for studying hydrodynamic expansion features of both single and colliding plasmas. Synchronization of the laser and ICCD camera was achieved with the aid of a programmable timing generator (PTG) and a fast photodiode was used to monitor the onset of each laser pulse. The flux and the kinetic energy profiles of the ions emanating from single and colliding plasmas were measured using a FC detector. The FC detector was mounted $\sim$15 cm away from the target surface, 10° off-normal to one of the seed plasma laser focal lines and biased negatively for electron shielding. The FC was positioned such a way that plasma screening effect can be monitored by the presence of second plasma.

III. RESULTS AND DISCUSSION

A. ICCD fast imaging

The laser intensity used for generating each seed plasma was $\sim 8.3 \times 10^8$ W cm^{-2} and hence it is expected that plumes emit predominantly in the visible region of the electromagnetic spectrum. Fast photography employing an ICCD camera was used for studying hydrodynamic expansion of the plumes and its collision features. Fast imaging provides two-dimensional snap shots of the three-dimensional expansion of the plume[27,28] and is a very useful diagnostic technique for understanding the colliding plasmas propagation hydrodynamics and stagnation. We used different target materials (C, Al, Mo, W) for this study to get a better understanding of when and where interpenetration or stagnation happens at the colliding interface.[29] In laser produced plasmas, the physical and chemical properties[30,31] of the target are one of the governing factors determining the ion charge state, velocity, particle density, etc. Hence, depending upon the target material, the generated plume's ion emission features (velocity, flux) as well as plasma properties (temperature, density) will vary even at constant laser intensity. In this work, a hemi-circular target was used and laser beams were focused in such a way that the seed plasmas came to a material focus at the center of the hemi-circle. Figs. 2–5 give typical time-resolved images for W, Mo, Al, and C single and colliding plasmas. All these images are spectrally integrated in the spectral region 350–800 nm, while each image is obtained from a single laser shot and normalized to its maximum intensity for easier intercomparison. The images of both single and colliding plasmas were taken in vacuum with a gate width of 10% of respective gate delay. The selection of 10% gate width with respect to gate delay is for compensating the reduction in plasma intensity with time.

The single plume images shown in Figs. 2–5 clearly show that the hemisphere target geometry leads to focusing

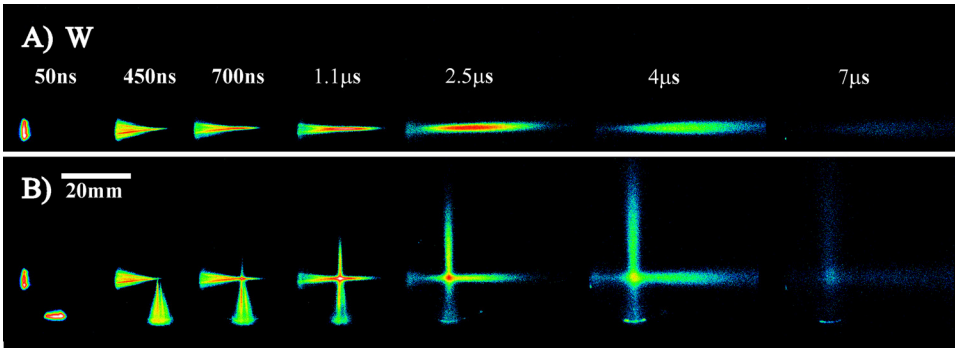

FIG. 2. Time-resolved images of (A) W single and (B) colliding plasma plumes emission in the visible spectral range (350–800 nm). The laser intensity used at each focus was $\sim 8.3 \times 10^8$ W cm^{-2}. Each image was recorded from a single laser shot and normalized to its maximum intensity.

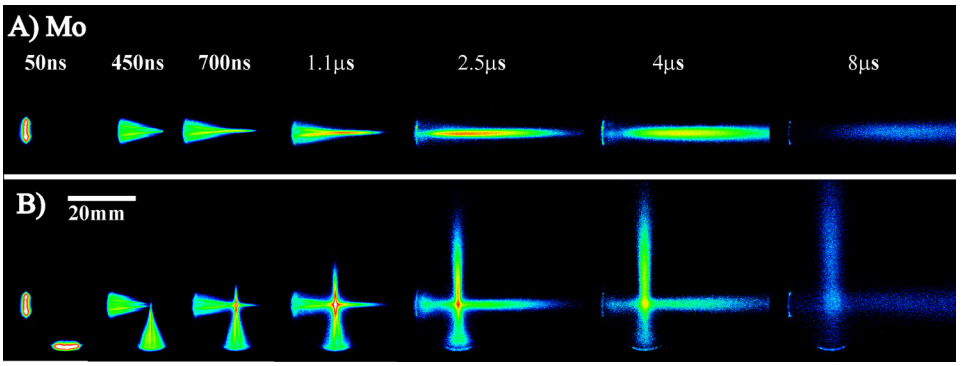

FIG. 3. Time-resolved images of (A) Mo single and (B) colliding plasma plumes emission in the visible spectral range (350–800 nm). The laser intensity used at each focus was $\sim 8.3 \times 10^8$ W cm^{-2}.

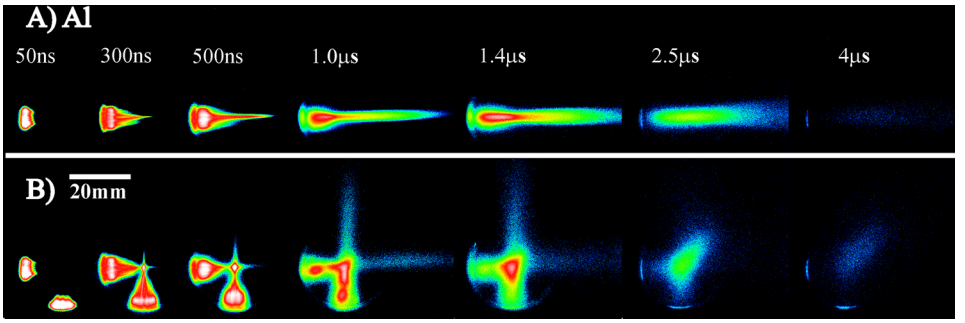

FIG. 4. Time-resolved images of (A) Al single and (B) Al colliding plasma plumes. The images are spectrally integrated in the visible spectral range (350–800 nm). The laser intensity used at each focus was $\sim 8.3 \times 10^8$ W cm^{-2}.

of the plasma at the hemisphere focal point. In the present experiments, we used a line focus method on a curved target where each seed plasma contracts in the orthogonal direction as it propagates normal to the target tangent resulting in the observation of seed plasma plume focusing. The present experimental setup gives detailed information about interpenetration and stagnation in the colliding plasma region. Figs. 2 and 3 show that the W and Mo seed plasmas focus and collapse at the center of target at a time delay of ~450 ns. Both interpenetration and stagnation are visible in the colliding plasma experiments for Mo and W targets, although the stagnation layer is found to be weak (bright spot at the focal point). It indicates that seed plasmas of W and Mo expand freely and interpenetrate each other in vacuum with a relatively small degree of stagnation (designated "soft" stagnation here) at the collapsing point.

The colliding plasmas obtained from Al targets (Fig. 4) showed contrasting behavior compared to W or Mo colliding

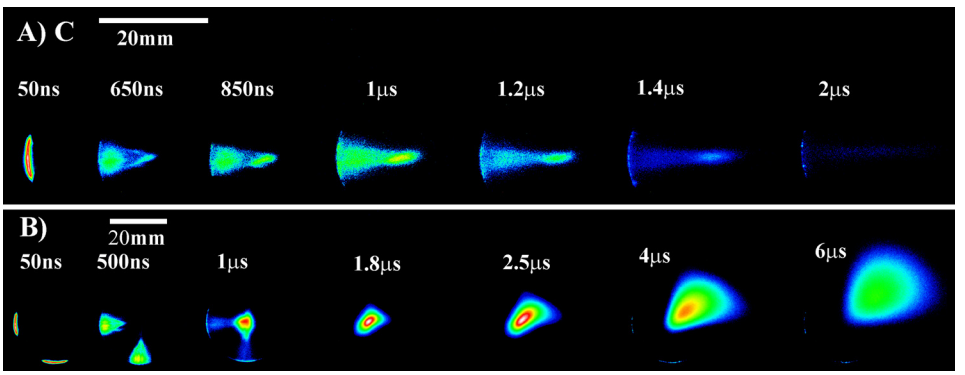

FIG. 5. Time-resolved images of (A) C single and (B) C colliding plasma plumes emission. The images are spectrally integrated in the visible spectral range (350–800 nm). The laser intensity used at each focus was $\sim 8.3 \times 10^8$ W cm^{-2}. Please note that the time scales and spatial scales given in this figure are different for single and colliding plumes.

schemes. In the case of aluminum, the stagnation regime is found to be brighter and interpenetration is significantly reduced compared to the high-Z seed plasmas. The colliding plasmas also appeared at earlier times (~300 ns) compared to W or Mo plasmas (~450 ns). This can be explained by considering the differences in the velocities of fast moving ions. The kinetic energy of the laser plasma ions scales inversely with the square root of the atomic mass.[32] At later times, the Al colliding region appears to move slowly at ~45° with respect to seed plasma stream direction and this can be understood by considering the changes in momentum. Fig. 5 shows time-resolved images for carbon single and colliding plasmas, respectively. The ICCD images shown in Fig. 5 clearly show an intense stagnation at the colliding plasma plane in the center of the target geometry without any seed plasma interpenetration ("hard" stagnation). The colliding effects of carbon plasmas were found to significantly enhance the emission persistence from ~2 μs to ~8 μs by confining the seed plasma expansion.

Comparing the colliding plasma schemes for all materials studied, interpenetration is most prominent for high-Z targets, while stagnation is dominant for low-Z targets. When two streaming plasmas collide, various interactions can arise depending upon the ion velocity, density, and charge state. These may be of a collisionless type, in which case collective plasma effects occur, or they are collision-dominated type. Depending upon the collisionality of the plasmas, varying amounts of interpenetration are expected. Our studies here have shown that interpenetration and stagnation of collapsing plasmas are strongly dependent on the atomic mass, the high-Z targets like W and Mo showing greater interpenetration, while low-Z material such as C shows plasma stagnation with minimal interpenetration for the laser parameters studied here. The degree of interpenetration is determined by the seed plasmas relative velocity and density. The interpenetration or stagnation (hard or soft) at the colliding interface is determined by the collisionality parameter, which is given by[3]

$$\xi = D/l_{ii}, \tag{1}$$

where D is the separation between the two seed colliding plasmas and l_{ii} is the ion–ion mean free path given by[33]

$$l_{ii} = \frac{4\pi\varepsilon_\circ^2 m_i^2 v_{12}^4}{e^4 Z^4 n_i \ln\wedge_{1\to 2}}, \tag{2}$$

where $\varepsilon_\circ$ is the free space permittivity, m_i is the ion mass, v_{12} is the relative incoming seed plasma ion velocity, e is the electronic charge, Z is average ionic charge state of the plasma, n_i is the ion density, and $\ln\wedge_{1\to 2}$ is the Coulomb logarithm. Based on this equation, the interpenetration and stagnation properties of seed plasmas are governed by ion velocity and density. Hence, we evaluated the kinetics of ion emission from these plasmas using Faraday cups for getting further insight.

B. Ion emission analysis

The fast gated imaging analysis showed that the plasmas generated by low-Z materials stagnate in the collision region, while the high-Z metal plasmas interpenetrate. So we evaluated the ion flux as well as velocities of single plasmas and the attenuation of the ion signal due to plasma shielding using a Faraday cup. Ion analysis employing FCs is one of the easiest technique to implement[1,34,35] and it provides significant information of the charge-integrated ion flux, ion temporal profiles, and hence kinetic energy distributions. Ion emission temporal-profiles from single and colliding plasmas of the four targets used, viz., W, Mo, Al, and C were collected and are given in Figs. 6 and 7. The ion signals shown include the signals collected by the FC using a single laser beam to generate a seed plasma and collect ions from one of the horizontally expanding seed plasmas in the presence of second plasma. Previous studies showed that bulk of the plasma ions from ns LPP are emitted in a cone with an angle ~45° with respect to target normal.[36] Typically, the angular distribution of ions in laser generated plasmas from solid targets follows an approximately $\cos^n$ function, where the value of n increases with the charge state and decreases with the atomic mass.[37] Hence, the ion contribution from the second seed plasma will be negligible considering the FC detector is positioned approximately orthogonal to the second

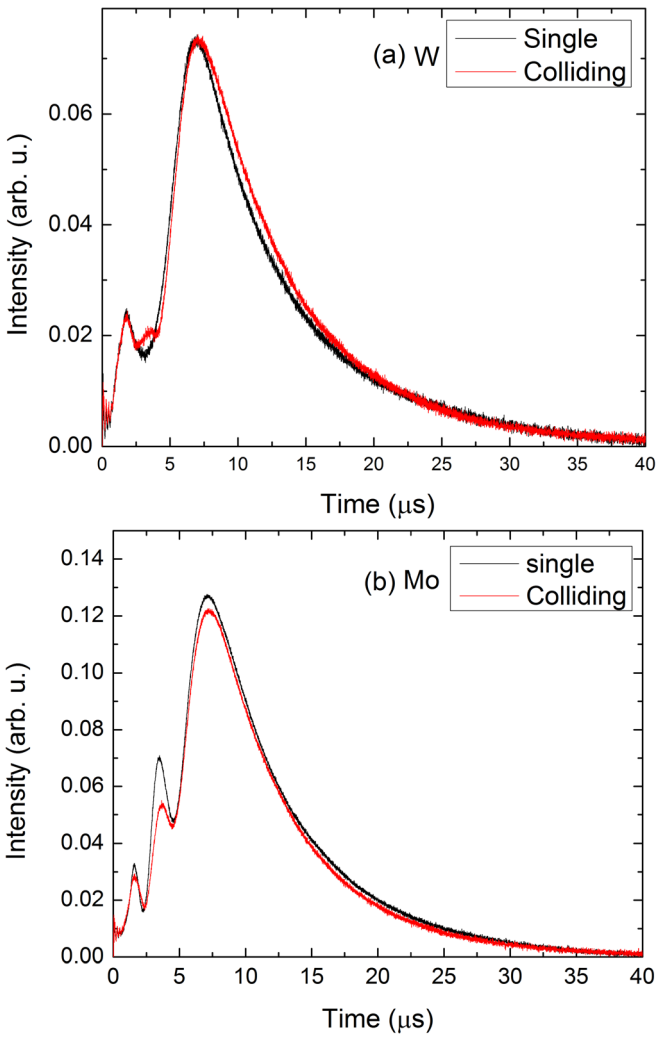

FIG. 6. Time of flight ion signal obtained from (a) W and (b) Mo single and colliding plasma schemes. To obtain ion signals, the FC was positioned 15 cm from the seed plasma target normal and the FC was biased negatively for screening electrons.

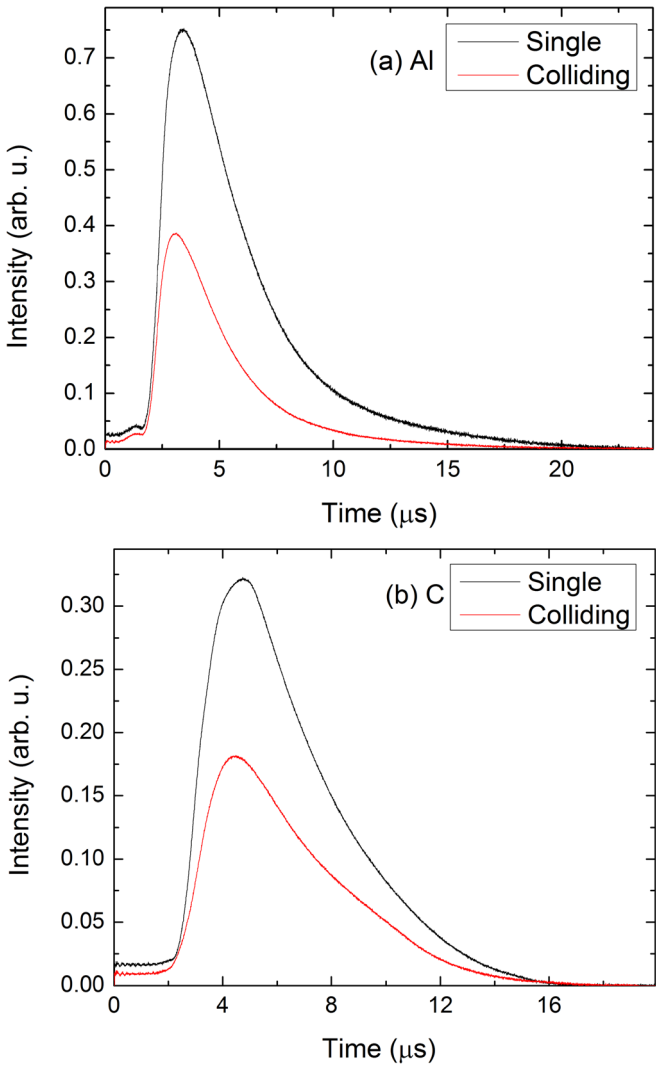

FIG. 7. Time of flight ion signal obtained from (a) Al and (b) C single and colliding plasma schemes are given. To obtain ion signals, the FC was positioned 15 cm from the seed plasma target normal and the FC was biased negatively for screening electrons.

seed plasma's expansion direction (Fig. 1(b)). The ion emission from the seed plasmas is expected to be significantly reduced if stagnation occurs.

The ion analysis using the FC showed that the ion flux decreased with increasing atomic mass of metal targets (Al, Mo, and W) for the laser parameters used in this study. On the other hand, the estimated velocities for Al, Mo, and W metal ions are 4.4×10^6 cm/s, 2.2×10^6 cm/s, and 2×10^6 cm/s, respectively, and hence showed a decreasing tendency with increasing atomic number. A similar trend has been reported previously and noticed that the flux and velocity of ions depend on atomic mass as well as sublimation energy.[32] The ions emanating from C targets moved with a velocity $\sim 3.25 \times 10^6$ cm/s. The kinetic ion current profiles also showed distinct differences between the high-Z and low-Z materials. Low-Z materials such as Al and C exhibited single peak ion distributions, while for high-Z materials (W and Mo) multiple peak structures. The multiple peak structure in the ion temporal profiles exhibited by high-Z elements was also reported recently[32] and was explained to be due to the presence of a higher flux of fast prompt electrons[38] in the case of high-Z targets compared to low-Z elements. The presence of fast prompt electrons leads to the generation of higher KE ions due to space charge effects that can accelerate a portion of highly charged ions.[32]

Plasma screening effects can be understood by comparing the FC signals obtained from the seed and dual plasmas. The ion time-of-flight signals showed that the plasma screening effects decrease with increasing atomic number/mass, which is in agreement with the recorded ICCD images. Comparing the single and dual plasma ion intensities, we noticed that W and Mo have almost similar signals in terms of shape, intensity, and delay time. This indicates that both seed plasma ions are interpenetrating without undergoing significant collisions. Hence, the single plasma ion intensity and delay time did not change significantly with the introduction of the other seed plasma. In contrast, this is not true for the case of aluminum and carbon plasmas. In the case of aluminum and carbon, the ion signals for the single seed plasmas were attenuated in the presence of the second plasma. Moreover, the observed peak velocity of the ions is higher in the presence of screening plasma. For example, the peak velocities of Al ions in the absence and presence of screening plasma are 4.4×10^6 cm/s and 5×10^6 cm/s, respectively, while these values for the C target are 3.25×10^6 cm/s and 3.4×10^6 cm/s, respectively. It shows that the faster ions from the seed plasmas are interpenetrating, while the slower ions with higher density are decelerating in the vicinity of the collision plane. According to Eqs. (1) and (2), the collisionality parameter varies inversely with ion-ion mfp, which scales as v^4/n_i. This implies that for low relative velocity and high-density seed plasmas, little or no penetration is expected and plasma species accumulation at the colliding interaction zone occurs forming the stagnation layer. The ion data analysis showed that the maximum probable velocity of the plasma ions is increasing with decreasing atomic weight. However, the ion flux values recorded for seed plasmas are significantly higher for low-Z materials compared to high-Z targets. This may lead to plasma stagnation in the case of low-Z targets such as C and Al, while more interpenetration can be expected for high-Z materials such as W and Mo.

C. Space-resolved optical emission spectroscopy

The ICCD imaging and ion profiles indicate the appearance of an intense stagnation region in the case of colliding carbon plasmas at the collision front. This leads us to investigate the properties of carbon stagnation layer using optical spectroscopy. Wavelength dispersed spectral images were recorded by rotating and focusing the self-emission images onto the vertical slit of the spectrograph for both seed and colliding carbon plumes by using a dove prism. Typical wavelength dispersed spectral images obtained from seed plasmas and the stagnation layer are given in Fig. 8. These spectral images were recorded from the center of the single plume or from the center of the stagnation layer along their expansion directions. The spectral details obtained from seed and colliding plasmas for distances of 1.5 mm and 15 mm

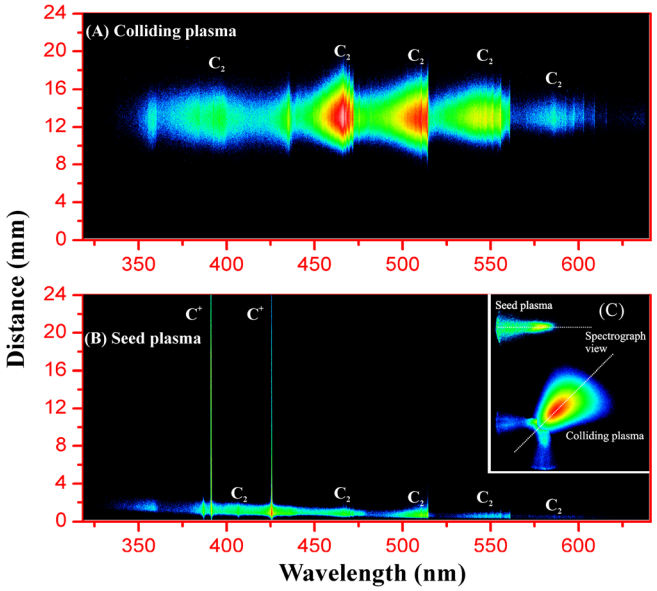

FIG. 8. Wavelength dispersed images of (A) colliding and (B) seed plasmas are shown. The spectrograph view position of seed and stagnation plasma overlayed on ICCD image is shown in (C). These spectra were obtained with a 600 g/mm grating providing a reciprocal linear dispersion of 3.2 nm/mm. An integration time of 2 μs and 100 μm spectrograph slit width were used.

with respect to the target are given in Fig. 9. The spectrometer slit direction is marked in Fig. 8(c) (inset in Fig. 8(b)) for both single and colliding plasmas. The Swan band emission corresponding to transitions between the $d^3\Pi_g$ and $a^3\Pi_u$ electronic states[39,40] of the C_2 molecule for $\Delta\nu = -1$, 0, 1, and 2 are clearly visible in this figure. These spectra were recorded with an integration time of 2 μs and a slit width of 100 μm.

The spectral images contained in Fig. 8 show that single plasma emission is very spatially confined, with a small extent (<3 mm) largely constituted by C_2 Swan band radiation. The exception is singly ionized species that exhibit bright line emission features at distances extending up to 25 mm from the target surface. This indicates that most of the emission contained in the ICCD images of seed carbon plasmas at farther distances originates from ionic species. However, the space and spectrally resolved spectra from the stagnation region showed only the presence of intense C_2 bands; hence ions were presumably absent or at least present in quantities too low to be detected against the bright C_2 emission.

The collisions in the stagnation region, which starts to form at large distances from the laser spot (at around ~14 mm away from the target surface) lead to the conversion of a significant part of the seed plasmas kinetic energy to stagnation layer thermal energy. The ensuing radiation losses from the bright stagnation layer eventually cool it down so that it becomes an environment conducive to C_2 formation.[26,27]

The electron temperature and density estimates for the seed plasmas were made by employing optical emission spectroscopy. However, this method is not usable for estimating plume parameters of stagnation layer due to the absence of line emission. The Saha-Boltzmann method was

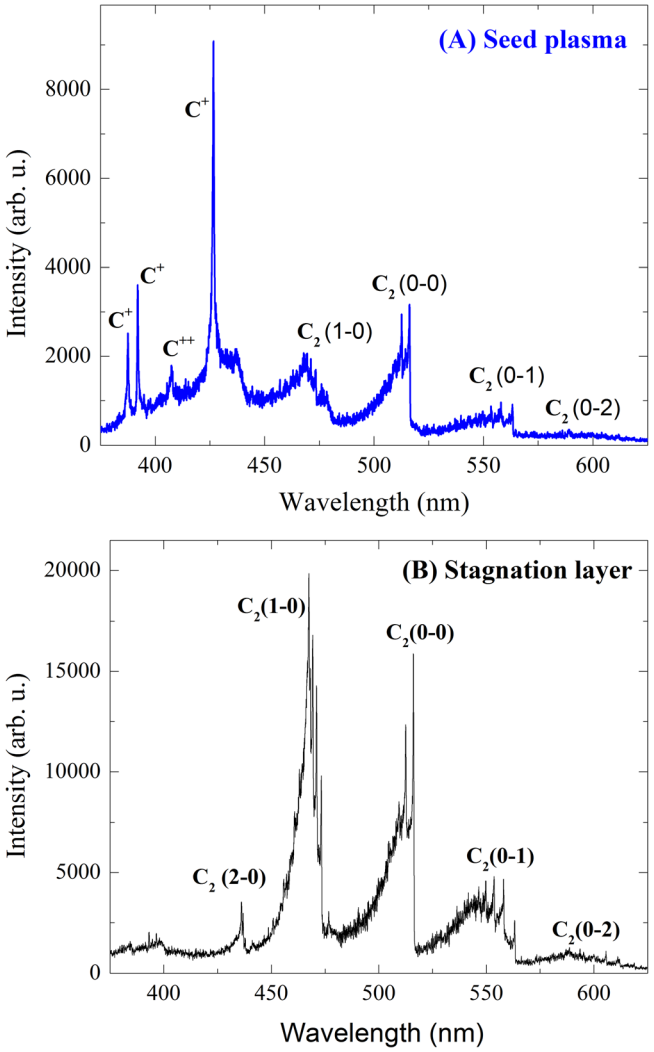

FIG. 9. An optical spectrum recorded from the seed plasma at a spatial position of 1.5 mm is shown in (A). In (B), the spectral features obtained from the stagnation region are shown (spatial location 15 mm). The spectra were obtained from Fig. 8 and the integration time used was of 2 μs.

used to estimate the temperature by using line intensities of C^{++} (407 nm) and C^+ (426.7 nm), while the Stark broadened line profile of C^+ at 426.7 nm was used for the density estimate. The spatial variation of electron temperature and density are given in Fig. 10 for a carbon seed plasma. Due to plasma expansion, the electron density and temperature were found to decrease with increasing distance from the target surface. It can be seen from this figure that electron density decreases more rapidly with distance from the target surface than temperature. For example, the recorded temperature at 0.5 mm is 2.70 eV and decreases to 2.54 eV at 3 mm from the target or just 6%, while the corresponding figures for density are just above $1.8 \times 10^{16}\,cm^{-3}$ and just below $0.6 \times 10^{16}\,cm^{-3}$ or by a factor of 3. The slight reduction in temperature could be caused by confinement of the seed plasma due to plasma collapse.

Because of the lack of neutral or ionic lines, it was not possible to estimate the electron density and temperature in the stagnation region. However, the absence of these lines also indicates that the stagnation layer seen in the collapsing experimental scheme has a low electron temperature. Using

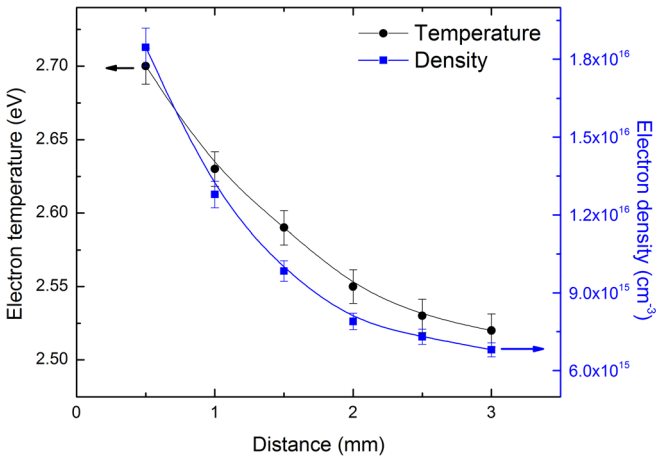

FIG. 10. Spatial evolution of electron density and temperature of carbon seed plasma estimated using optical emission spectroscopy. The Saha-Boltzmann method is used for the temperature estimate. The electron density was obtained from the Stark broadened profiles and they were recorded using the 1800 g/mm grating of the spectrograph. An integration time of 2 μs and 30 μm spectrograph slit width were used.

the summation rule of the vibrational intensities of different Swan bands,[41] the stagnation layer C_2 vibrational temperature was estimated[27] from high resolution emission spectra. The spatial evolution of the vibrational temperature at the stagnation layer is shown in Fig. 11. The maximum vibrational temperature of ~0.95 eV is observed at a distance of 15 mm from the target. As the ICCD images show, the seed plasmas collapse and the plasma constituents from each plume accumulate at the collision plane followed by further collisions between the following plume material and full stagnation layer formation. The stagnation layer is found to expand or grow outwards along a direction of 45° with respect to seed plasma expansion axis. This causes the C_2 vibrational temperature to peak at around 15 mm, where most of the seed plasma species are focused leading to the brightest C_2 emission at the center of the curved target.

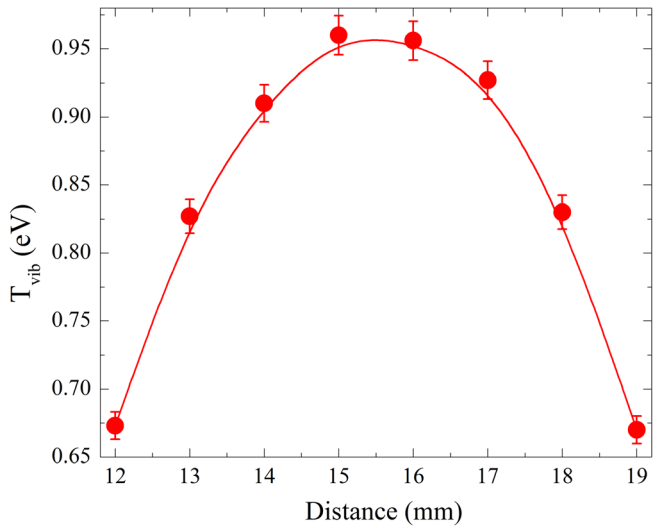

FIG. 11. Spatial evolution C_2 vibrational temperature in the stagnation layer of carbon colliding plasmas. These measurements were obtained using the 600 g/mm grating of the spectrograph. An integration time of 2 μs and 100 μm spectrograph slit width were used.

The laser produced carbon colliding plasmas showed brightest stagnation layer formation and ICCD images showed that interpenetration is minimal. However, the FC signal showed a part of the fast ions interpenetrated without collisions or plasma screening. It indicates that the faster ions escape the interaction zone before the formation of stagnation layer. The emission from the stagnation layer found in carbon colliding plasmas is mainly due to C_2 emission. It is well known that the C_2 plays a prominent role in the formation of carbon clusters and nanotubes.[23,27] So the plasma collision at the center of fusion chambers with the use of C as a PFC may lead to rapid cooling of the plumes and generate debris in the form of clusters and nanotubes that can hinder the timely chamber clearing required for higher repetition rate.

IV. CONCLUSIONS

We investigated plasma stagnation and interaction effects in colliding laser-produced plasmas. The purpose of this research was to develop a better understanding of collision physics among plasmas in fusion reactors and subsequent screening effects and formation of debris. The single plume and stagnation layer dynamics of candidate fusion wall materials, viz., carbon and tungsten, and other materials such as aluminum and molybdenum were investigated using a multitude of plasma diagnostic tools. Fast ICCD images indicated that molybdenum and tungsten LPPs interpenetrate each other at the colliding interface, while aluminum seed plasmas initially interpenetrate and later stagnate. In contrast, the carbon target colliding scheme showed very intense stagnation in the collision region that increased significantly the persistence of plasma emission. The ion profiles indicate that colliding plasmas interpenetration exhibited by heavy metals, Mo and W, is due to lower ion density. This reduces the ion interaction time and probability of collisions. In contrast, aluminum and carbon ion profiles showed higher ion density helping to create a higher collision frequency and the concomitant formation of the stagnation layer.

Spectroscopic analysis of the stagnation layer formed by carbon plumes showed the increased persistence of emission from the stagnation layer evidenced by intense C_2 swan band emission. The stagnation layer formed at the collision plane is found to expand in a direction 45° with respect to seed plasma expansion direction. This is explained by changes in the momentum vector caused by plume collisions. The estimated temperature and density of seed plasmas showed reductions in both parameters with distance from the target, though the temperature decrease was moderate probably caused by plasma focusing. The vibrational temperature analysis of molecular band emission from the stagnation layer exhibited a temperature of ~0.95 eV, which is significantly lower than the estimated temperature of the seed plasmas.

In the context of fusion reactor chamber clearing, the present results indicate that under similar laser irradiation conditions, for the PFC materials, tungsten and carbon, colliding plasmas showed different characteristics. While tungsten plumes interpenetrate each other at the collision interface for the laser parameters used in this study, carbon

colliding plumes formed a strong stagnation layer, which could be a source of nanoparticles and plasma aerosols.

ACKNOWLEDGMENTS

This work was partially supported by the U.S. National Science Foundation PIRE and Japan JSPS PIRE programs. Participation of DCU was supported by Science Foundation of Ireland under Grant No. 12/IA/1742.

[1]P. Hough, P. Hayden, C. Fallon, T. J. Kelly, C. McLoughin, P. Yeates, J. P. Mosnier, E. T. Kennedy, S. S. Harilal, and J. T. Costello, "Ion emission in collisions between two laser-produced plasmas," J. Phys. D **44**, 355203 (2011).
[2]E. Irissou, F. Vidal, T. Johnston, M. Chaker, D. Guay, and A. N. Ryabinin, "Influence of an inert background gas on bimetallic cross-beam pulsed laser deposition," J. Appl. Phys. **99**, 034904 (2006).
[3]P. W. Rambo and J. Denavit, "Interpenetration and ion separation in colliding plasmas," Phys. Plasmas **1**, 4050–4060 (1994).
[4]P. Yeates, C. Fallon, E. T. Kennedy, and J. T. Costello, "Charge resolved electrostatic diagnostic of colliding copper laser plasma plumes," Phys. Plasmas **18**, 103104 (2011).
[5]D. D. Ryutov, N. L. Kugland, M. C. Levy, C. Plechaty, J. S. Ross, and H. S. Park, "Magnetic field advection in two interpenetrating plasma streams," Phys. Plasmas **20**, 032703 (2013).
[6]S. L. Gupta, P. K. Pandey, and R. K. Thareja, "Dynamics of laser ablated colliding plumes," Phys. Plasmas **20**, 013511 (2013).
[7]C. S. Ake, R. S. de Castro, H. Sobral, and M. Villagran-Muniz, "Plume dynamics of cross-beam pulsed-laser ablation of graphite," J. Appl. Phys. **100**, 053305 (2006).
[8]T. Kono, A. Ishikawa, S. Misaki, A. Sunahara, S. Tanaka, T. Yabuuchi, Y. Hirooka, and K. A. Tanaka, "Material dependence on plasma shielding induced by laser ablation," Plasma Fusion Res. **7**, 2405065 (2012).
[9]K. A. Tanaka, A. Hassanein, Y. Hirooka, T. Kono, S. Misaki, T. Ohishi, A. Sunahara, and S. Tanaka, "Carbon plume stagnation: Platform for vapor shield study," Fusion Sci. Technol. **60**, 329–333 (2011).
[10]E. Leboucher-Dalimier, P. Angelo, P. Gauthier, P. Sauvan, A. Poquerusse, H. Derfoul, T. Ceccotti, C. A. Back, T. D. Shepard, E. Forster, I. Uschmann, and M. Vollbrecht, "X-ray spectroscopy and imaging of hot dense plasma created by colliding foils. Simulation of spectra," J. Quantitative Spectrosc. Radiat. Transfer **58**, 721–735 (1997).
[11]R. T. Eagleton, J. M. Foster, P. A. Rosen, and P. Graham, "One-dimensional time resolved soft x-ray imaging of colliding plasmas in a laser heated cavity," Rev. Sci. Instrum. **68**, 834–837 (1997).
[12]M. Purvis, J. Grava, J. Filevich, M. C. Marconi, J. Dunn, S. J. Moon, V. N. Shlyaptsev, E. Jankowska, and J. J. Rocca, "Dynamics of converging laser-created plasmas in semicylindrical cavities studied using soft x-ray laser interferometry," Phys. Rev. E **76**, 046402 (2007).
[13]S. S. Harilal, C. V. Bindhu, and H. J. Kunze, "Time evolution of colliding laser produced magnesium plasmas investigated using a pinhole camera," J. Appl. Phys. **89**, 4737–4740 (2001).
[14]H. Luna, K. D. Kavanagh, and J. T. Costello, "Study of a colliding laser-produced plasma by analysis of time- and space-resolved image spectra," J. Appl. Phys. **101**, 033302 (2007).
[15]A. Tselev, A. Gorbunov, and W. Pompe, "Cross-beam pulsed laser deposition: General characteristic," Rev. Sci. Instrum. **72**, 2665–2672 (2001).
[16]S. Witanachchi, A. M. Miyawa, and P. Mukherjee, "Highly ionized carbon plasma generation by dual-laser ablation for diamond-like carbon film growth," in MRS Proceedings **617**, J3.6.1–J.3.6.6 (2000).
[17]S. S. Harilal, C. V. Bindhu, V. P. Shevelko, and H. J. Kunze, "Charge-exchange collisions in interpenetrating laser-produced magnesium plasmas," Laser Part. Beams **19**, 99–103 (2001).
[18]S. S. Harilal, C. V. Bindhu, V. P. Shevelko, and H. J. Kunze, "XUV diagnostics of colliding laser-produced magnesium plasmas," J. Phys. B **34**, 3717–3726 (2001).
[19]A. S. Wan, T. W. Barbee, R. Cauble, P. Celliers, L. B. DaSilva, J. C. Moreno, P. W. Rambo, G. F. Stone, J. E. Trebes, and F. Weber, "Electron density measurement of a colliding plasma using soft-x-ray laser interferometry," Phys. Rev. E **55**, 6293–6296 (1997).
[20]R. C. Elton, D. M. Billings, C. K. Manka, H. R. Griem, J. Grun, B. H. Ripin, and J. Resnick, "Spectroscopic diagnostics in a colliding-blast-wave experiment," Phys. Rev. E **49**, 1512–1519 (1994).
[21]H. Sato, Y. Hirooka, K. A. Tanaka, and K. Ishihara, "Dynamics of colliding ablation plumes," J. Plasma Fusion Res. Ser. **9**, 432–435 (2010).
[22]T. J. Renk, C. L. Olson, T. J. Tanaka, M. A. Ulrickson, G. A. Rochau, R. R. Peterson, I. E. Golovkin, M. O. Thompson, T. R. Knowles, A. R. Raffray, and M. S. Tillack, "IFE chamber dry wall materials response to pulsed X-rays and ions at power-plant level fluences," Fusion Eng. Des. **65**, 399–406 (2003).
[23]Y. Hirooka, T. Oishi, H. Sato, and K. A. Tanaka, "Aerosol formation and hydrogen co-deposition by colliding ablation plasma plumes of carbon," Fusion Sci. Technol. **60**, 804–808 (2011).
[24]Y. Hirooka, K. A. Tanaka, H. Sato, K. Ishihara, and A. Sunahara, "Laboratory experiments on cluster/aerosol formation by colliding ablation plumes," J. Phys. Conf. Ser. **244**, 032033 (2010).
[25]Y. Hirooka, N. Omoto, T. Oishi, and K. A. Tanaka, "Aerosol formation and hydrogen co-deposition by colliding ablation plasma plumes of lithium and lead," Fusion Eng. Des. **87**, 1760–1764 (2012).
[26]K. F. Al-Shboul, S. S. Harilal, and A. Hassanein, "Gas dynamic effects on formation of carbon dimers in laser-produced plasmas," Appl. Phys. Lett. **99**, 131506 (2011).
[27]K. F. Al-Shboul, S. S. Harilal, and A. Hassanein, "Emission features of femtosecond laser ablated carbon plasma in ambient helium," J. Appl. Phys. **113**, 163305 (2013).
[28]S. S. Harilal, M. P. Polek, and A. Hassanein, "Jetlike emission from colliding laser-produced plasmas," IEEE Trans. Plasma Sci. **39**, 2780–2781 (2011).
[29]A. Yogo, K. Sato, M. Nishikino, M. Mori, T. Teshima, H. Numasaki, M. Murakami, Y. Demizu, S. Akagi, S. Nagayama, K. Ogura, A. Sagisaka, S. Orimo, M. Nishiuchi, A. S. Pirozhkov, M. Ikegami, M. Tampo, H. Sakaki, M. Suzuki, I. Daito, Y. Oishi, H. Sugiyama, H. Kiriyama, H. Okada, S. Kanazawa, S. Kondo, T. Shimomura, Y. Nakai, M. Tanoue, H. Sasao, D. Wakai, P. R. Bolton, and H. Daido, "Application of laser-accelerated protons to the demonstration of DNA double-strand breaks in human cancer cells," Appl. Phys. Lett. **94**, 181502 (2009).
[30]G. Baraldi, A. Perea, and C. N. Afonso, "Dynamics of ions produced by laser ablation of several metals at 193 nm," J. Appl. Phys. **109**, 043302–043306 (2011).
[31]A. Sunahara and K. A. Tanaka, "Atomic number Z dependence of dynamics of laser-ablated materials," Fusion Eng. Des. **85**, 935–939 (2010).
[32]F. Nazar, S. S. Harilal, H. Ding, and A. Hassanein, "Kinetics of ion and prompt electron emission from laser-produced plasma," Phys. Plasmas **20**, 073114 (2013).
[33]J. Dardis and J. T. Costello, "Stagnation layers at the collision front between two laser-induced plasmas: A study using time-resolved imaging and spectroscopy," Spectrochim. Acta Part B: Atom. Spectrosc. **65**, 627–635 (2010).
[34]R. Janmohamed, G. Redman, and Y. Y. Tsui, "Space charge effects in faraday cup ion detectors," IEEE Trans. Plasma Sci. **34**, 455–459 (2006).
[35]D. Doria, A. Lorusso, F. Belloni, and V. Nassisi, "Characterization of a nonequilibrium XeCl laser-plasma by a movable Faraday cup," Rev. Sci. Instrum. **75**, 387–392 (2004).
[36]B. Verhoff, S. S. Harilal, and A. Hassanein, "Angular emission of ions and mass deposition from femtosecond and nanosecond laser-produced plasmas," J. Appl. Phys. **111**, 123304 (2012).
[37]A. Thum-Jager and K. Rohr, "Angular emission distributions of neutrals and ions in laser ablated particle beams," J. Phys. D: Appl. Phys. **32**, 2827–2831 (1999).
[38]F. Caridi, L. Torrisi, D. Margarone, and A. Borrielli, "Investigations on low temperature laser-generated plasmas," Laser Part. Beams **26**, 265–271 (2008).
[39]R. W. B. Pearse and A. G. Gaydon, *The Identification of Molecular Spectra* (Chapman and Hall, London, 1965).
[40]W. Weltner and R. J. Vanzee, "Carbon molecules, ions, and clusters," Chem. Rev. **89**, 1713–1747 (1989).
[41]G. Herzberg, "Spectra of diatomic molecules," in *Molecular Spectra and Molecular Structure* (Van Nostrand, New York, 1950).